Magneto-plasmonic heterodimers: Evaluation of different synthesis approaches

Received: 9 July 2021 | Revised: 1 October 2021 | Accepted: 11 October 2021

DOI: 10.1111/jace.18190

Journal of the American Ceramic Society

RESEARCH ARTICLE

Magneto-plasmonic heterodimers: Evaluation of different synthesis approaches

Marta Miola[1] | **Cristina Multari**[1] | **Doriana Debellis**[2] | **Francesco Laviano**[1] | **Roberto Gerbaldo**[1] | **Enrica Vernè**[1]

[1] Department of Applied Science and Technology, Politecnico di Torino, Torino, Italy

[2] Electron Microscopy Facility, Istituto Italiano di Tecnologia, Genova, Italy

Correspondence
Politecnico di Torino, Department of Applied Science and Technology, Politecnico di Torino, Italy, Corso Duca degli Abruzzi, 24 - 10129 (Torino) Italy.
Email: marta.miola@polito.it

Abstract

Nanomedicine has gained huge attention in recent years with new approaches in medical diagnosis and therapy. Particular consideration has been devoted to the nanoparticles (NPs) in theranostic field with specific interest for magnetic and gold NPs (MNPs and GNPs) due to their peculiar properties under exposition to electromagnetic fields. In this paper, we aim to develop magneto-plasmonic heterodimer by combining MNPs and GNPs through a facile and reproducible synthesis and to investigate the influence of different synthesis parameters on their response to magnetic and optical stimuli. In particular, various syntheses were performed by changing the functionalization step and using or not a reducing agent to obtain stable NP suspensions with tailored properties. The obtained heterodimers were characterized through physical, chemical, optical, and magnetic analysis, in order to evaluate their size, shape, plasmonic properties, and superparamagnetic behavior. The results revealed that the shape and dimensions of the nanocomposites can be tuned by MNPs surface functionalization, as well as by the use of a reducing agent, giving rise to nanoplatform suitable for biomedical application, exploiting the gold absorbing peak in the specific gold absorbing range of GNPs, while maintaining the superparamagnetic behavior typical of the MNPs. The obtained nanocomposites can be proposed as potential candidates for cancer theranostics.

KEYWORDS

gold nanoparticles, magnetite nanoparticles, magneto-plasmonic heterodimers, tannic acid

1 | INTRODUCTION

In recent years, nanotechnology has received huge attention, with particular interest in the medical sector (nanomedicine),[1] with new approaches in the field of imaging, drug administration, and cancer treatment.[2,3] Nanomedicine aims to make medical diagnosis and therapy significantly more effective. In the theranostic field, nanoparticles (NPs) can be used, for example, to create alternative drug targeting systems in the body, as contrast agents in magnetic resonance imaging or in hyperthermic treatments for tumors.[4,5] In particular, the use of magnetic NPs (MNPs) in medical applications offers great potential in the therapeutic field as well as in in vitro and in vivo

diagnostics.[6–8] In fact, they possess unique magnetic properties that depend on their size, shape, structure, crystallinity, method of synthesis, dispersion, and surface chemistry.[9–11]

Also gold NPs (GNPs) received huge attention in biomedical field due to their high biocompatibility and their peculiar ability to scatter with visible light. In fact, owing to the surface plasmon resonance (SPR) effect, they can be exceptionally used as photosensitizers in photothermal therapy, since GNPs are able to transform the received light into thermal energy which could bring the cancer cells to apoptosis due to their high heat sensitivity.[12]

By combining MNPs and GNPs, it is possible to join the properties of these two nanomaterials by creating hybrid nanoplatforms. Different approaches have been proposed in literature to synthesize magneto-plasmonic nanoplatforms, that can be assembled into two strategies: (i) the separate synthesis of iron oxide NPs and GNPs and their subsequent combination using different linkers (e.g., molecule, polymers)[13–15]; (ii) the in situ reduction of GNPs directly on iron-oxide surface.[16–18] On the basis of procedure, different structures can be obtained, such as core/shell, core/satellite, or nanodumbells.[19]

In order to reduce the GNPs on iron oxide NPs surface, different strategies have been investigated, by exploiting several chelating and reducing agents.[12,20,21] Recently, the authors proposed a simple in situ reduction process of a soluble gold salt on (3-Aminopropyl)triethoxysilane (APTES)-functionalized magnetite NPs tailoring the molar ratio of the reagents, the pH and temperature of the process and avoiding the use of a specific reducing agent.[22] In an additional study published by the authors, hybrid gold-magnetite nanoplatforms was obtained through a facile and reproducible synthesis method in which tannic acid (TA) was used as eco-friendly reducing agent.[23] Another in situ reduction was proposed by Sood et al., in which gold-coated magnetite NPs were synthesized by reduction of gold chloride onto the iron oxide NPs surface, using ascorbic acid as reducing and capping agent.[20] Dizaji et al., proposed an environmentally friendly procedure to generate hybrid NPs by reducing Ag or Au ions directly on the MNPs surface by using plant extracts as reducing and stabilizing agents.[21]

The purpose of this work is the development of magneto-plasmonic heterodimer through a facile and reproducible synthesis and the investigation of the influence of synthesis parameters (e.g., the use of reducing agent and the synthesis steps sequence) on their response to magnetic and optical stimuli. In particular, different syntheses were investigated by changing the conditions of the functionalization step and using or not a reducing agent. Finally, the NPs were characterized through physical, chemical, optical, and magnetic analysis, in order to evaluate their size, shape, plasmonic properties, and superparamagnetic behavior.

2 | MATERIALS AND METHODS

2.1 | Synthesis of magnetite-based NPs

Magnetite-based NPs (MNPs) were produced by co-precipitation process as described in our previous articles.[22,24,25] Briefly, appropriate amount of 0.01 M $FeCl_2*4H_2O$ and 0.01 M $FeCl_3*6H_2O$ were mechanically mixed in bi-distilled in water to reach a stoichiometric ratio Fe^{2+}/Fe^{3+} of 1:2. To allow the formation of magnetic NPs, NaOH was added dropwise up to a pH = 10, and the solution was placed in an ultrasound bath for 20 min. Subsequently, MNPs were magnetically separated and washed using bi-distilled water. Then, MNPs were functionalized with citric acid (CA) to improve their dispersion in water. MNPs were suspended in a CA solution 0.05 M, the pH was adjusted at 5.2 by dropwise NH_4OH, and the suspension was placed 90 min at room temperature in orbital shaker (KS 4000i control, IKA) at 150 rpm to allow the deprotonation of two CA carboxylic groups and the bond to the -OH groups exposed by MNPs.[26] Afterward, MNPs were washed with bi-distilled water using an ultrafiltration device (Solvent Resistant Stirred Cells - Merck Millipore) and re-suspended in bi-distilled water. The pH of the suspension was fixed at 10.1 to induce the deprotonation of the third carboxylic group of CA, to reach MNPs dispersion through electrostatic stabilization. All chemicals were purchased from Sigma-Aldrich.

2.2 | Synthesis of magnetite-gold magneto-plasmonic heterodimer (M-A-Au)

CA-stabilized MNPs were functionalized with APTES to expose $-NH_2$ group and enhance the interaction between MNPs and GNPs.[22,27,28] MNPs were diluted in absolute ethanol and sonicated for few minutes; then two amounts of APTES were added, using an MNPs (ml)/APTES (μl) ratios of 0.3 and 0.09. The obtained suspensions were heated at 80°C and stirred at 150 rpm for 3 h; at the end of incubation, the functionalized MNPs were magnetically separated and centrifuged for three times at 7500 rpm for 20 min in a mixture of water:ethanol 1:1 in volume. Lastly, the pH of the suspension containing MNPs functionalized with APTES (M-A) was stabilized at about 5-6 by adding dropwise a diluted HNO_3 solution (0.05 ml of 6 M HNO_3 with 20 ml of ethanol), to induce a positive charge at the M-A surface, useful to the subsequent GNPs grafting.[27,28]

Colloidal GNPs were synthesized by reduction of soluble gold salt ($HAuCl_4$): 4 ml of $HAuCl_4$ (12.7 mM)

TABLE 1 List of parameters used in the various synthesis. (x) indicates the adopted reagents

	APTES (μl)	$HAuCl_4$	TA	$HAuCl_4$ + TA
Synthesis 1a	30	x		
Synthesis 2a	30			x
Synthesis 3a	30	x	x	
Synthesis 1b	100	x		
Synthesis 2b	100			x
Synthesis 3b	100	x	x	

was prepared, and the pH of the solution was adjusted at about 8 by adding NaOH 0.1 M, to allow the formation of gold hydroxide suspension ($Au(OH)_3$).[22] Subsequently, M-A-Au NPs were developed by grafting $Au(OH)_3$ colloidal seeds to the surface of M-A NPs and promoting their reduction to GNPs by using or not TAas reducing agent. The different adopted parameters are resumed in Table 1 ("x" indicates the adopted reagents for each synthesis).

For synthesis 1a and 1b, colloidal $Au(OH)_3$ seeds were directly mixed with M-A NPs suspension as described in our previous work,[22] but using two different APTES amount: 30 μl and 100 μl. For synthesis 2a, 3a, 2b, and 3b, a TA solution 1.25 mM was prepared, and a volume ratio of 10 between $Au(OH)_3$ colloidal solution and TA one was used. In synthesis 2a and 2b, $Au(OH)_3$ and TA were pre-mixed together 5 min at 70°C and added to the M-A NPs suspension, then all the mixtures were heated at a 70°C for 3 min under stirring. In synthesis 3a and 3b, $Au(OH)_3$ and TA solutions were added in sequence to the M-A NPs suspension and then heated at a 70°C for 5 min under stirring, as reported in a previous paper.[23] In order to remove the unreacted reagents and the excess of unloaded GNPs, all the suspensions were washed and centrifuged in bi-distilled water five times for 20 min at 40 rpm and re-suspended in bi-distilled water.

In Figure 1, a schematic representation of the three different synthesis procedures is reported.

2.3 | NPs characterization

All the obtained NPs were characterized from morphological and compositional point of view by means of scanning and transmission electron microscopy (STEM) (Merlin Gemini Zeiss) equipped with energy dispersive spectroscopy; TEM analysis was performed with an FEI

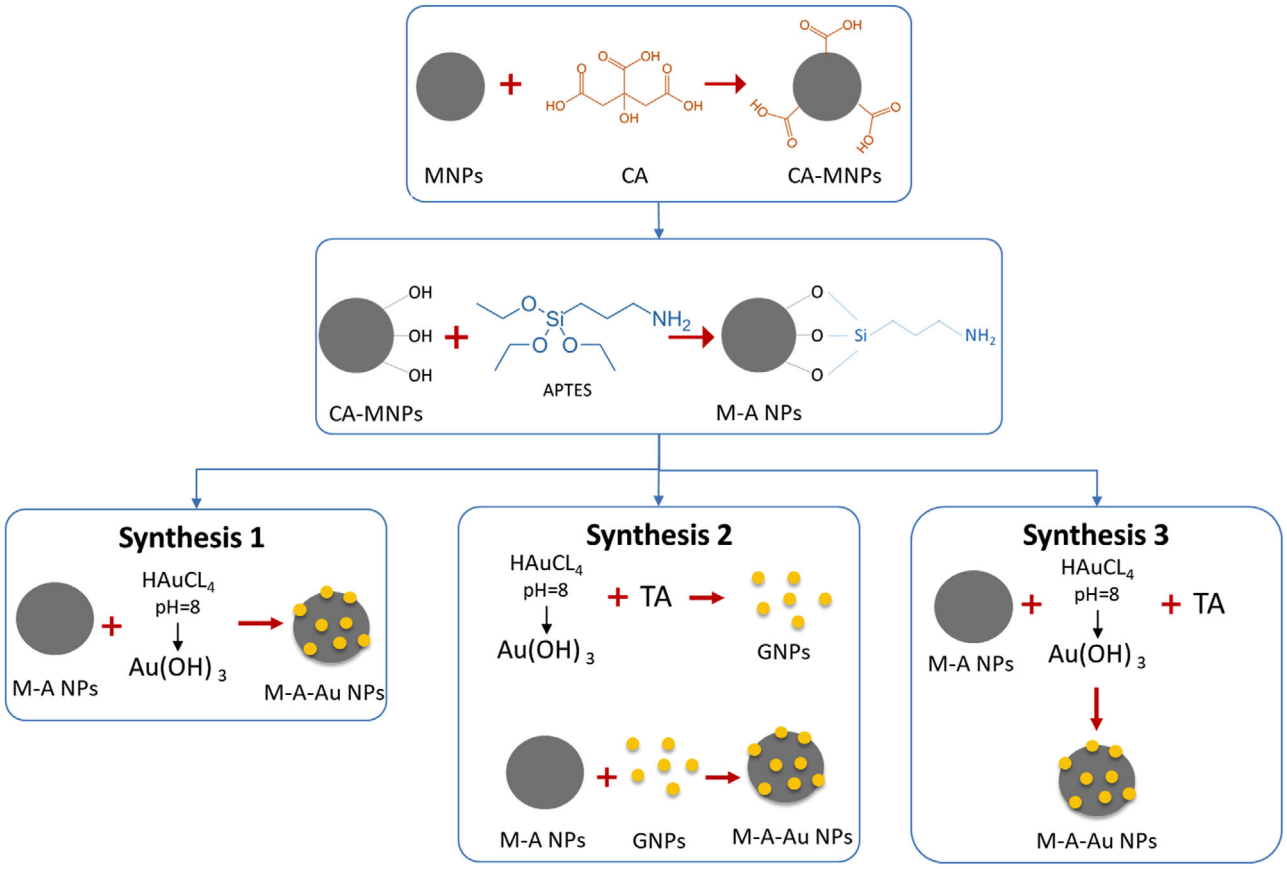

FIGURE 1 Schematic representation of the three synthesis procedures

TABLE 2 List of FT-IR spectra main peaks of magnetic nanoparticles (MNPs), citric acid (CA)-grafted MNPs, and M-A nanoparticles (NPs)

Sample	Wave-number (cm^{-1})	Assignments
MNPs	550	Fe_3O_4 stretching vibrational mode
MNPs + AC	550	Fe_3O_4 stretching vibrational mode
	1330	-CO asymmetric stretching
	1550	C = O vibration
	2660	CH_2 group stretching
MNPs+ AC + APTES	550	Fe_3O_4 stretching vibrational mode
	840	Si-O stretching
	1100	Si-O-Si stretching
	1550	N-H stretching vibration

Abbreviation: APTES, (3-Aminopropyl)triethoxysilane.

Tecnai F20 TWIN TEM with a Schottky emitter operated at 200 KV. For STEM and TEM analyses, a drop of diluted NPs suspension was deposited on a copper TEM grid with carbon film (SPI Supplies Brand Lacey Carbon Coated 200 Mesh Copper Grids – JEOL S.p.A.). FT-IR measurements were carried out using a Hyperion 2000 FT/IR (Tensor 27, Bruker Optics S.p.A, Ettlingen, Germany) from 4000 to 400 cm^{-1} and with 2 cm^{-1} resolution. OPUS software (v. 6.5, Bruker S.p.A) was used for instrumental control and spectral acquisition.

The optical properties of M-A-Au NPs were investigated by means of UV-Vis spectroscopy (PerkinElmer Lambda 950 spectrometer); the spectra were evaluated by measuring the suspension absorbance between 300 nm and 800 nm by using DI water as a reference.

The magnetic properties of all obtained NPs were investigated using a DC magnetometer/AC susceptometer (Lakeshore 7225) equipped with a Cryogen-Freemagnet at room temperature in quasi static condition. Magnetic hysteresis cycle measurements were performed using a magnetic field up to 800 kA/m, in order to estimate the main magnetic parameters of the materials and the influence of the synthesis process. To perform this analysis, the NPs were dried at room temperature for 24 h.

3 | RESULTS AND DISCUSSION

3.1 | Characterization of MNPs

Table 2 and Figure 2 show the list of the main peaks revealed from FT-IR analysis of MNPs, CA-stabilized MNPs, and M-A NPs. In all spectra, a peak at about 550 cm^{-1} ascribable to Fe_3O_4 stretching vibrational mode was observed[27]; the spectrum of CA-stabilized magnetite

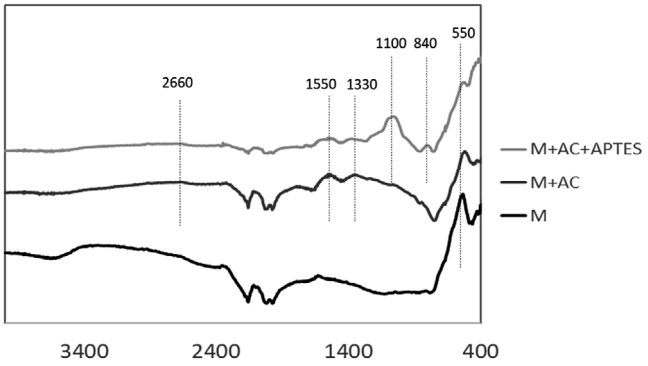

FIGURE 2 FT-IR spectra of magnetic nanoparticles (MNPs) (M), citric acid (CA)-grafted MNPs (M + AC) and M-A nanoparticles (NPs) (M + AC + (3-Aminopropyl)triethoxysilane [APTES])

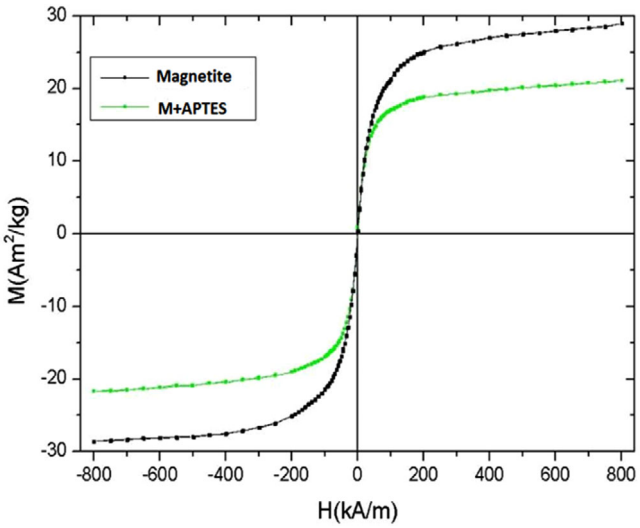

FIGURE 3 Hysteresis loop of magnetic nanoparticles (MNPs) (black curve) and M-A nanoparticles (green curve)

NPs shows a peak at about 1330 cm^{-1}, ascribable to the asymmetric stretching of -CO of CA-COOH group, at about 1550 cm^{-1} the peak due to the vibration of C = O of CA -COOH group and at 2660 cm^{-1} the stretching of CH_2 group.[29] The effective APTES functionalization was confirmed by the presence of the band at 840–1100 cm^{-1}, due to the Si-O and Si-O-Si stretching,[30] and by the peak at about 1550 cm^{-1} ascribable to the N–H stretching vibration,[31] which is indicative of the free amino group of APTES.

Figure 3 shows the magnetic measurements of MNPs and M-A NPs (functionalized with 100 μl APTES) which provide information on their magnetic response and the saturation magnetization. As it can be observed, both samples exhibit a superparamagnetic behavior, as confirmed by the magnetization versus applied magnetic field. Observing the curves, it is possible to notice that bare magnetite (MNPs) shows higher saturation magnetization in

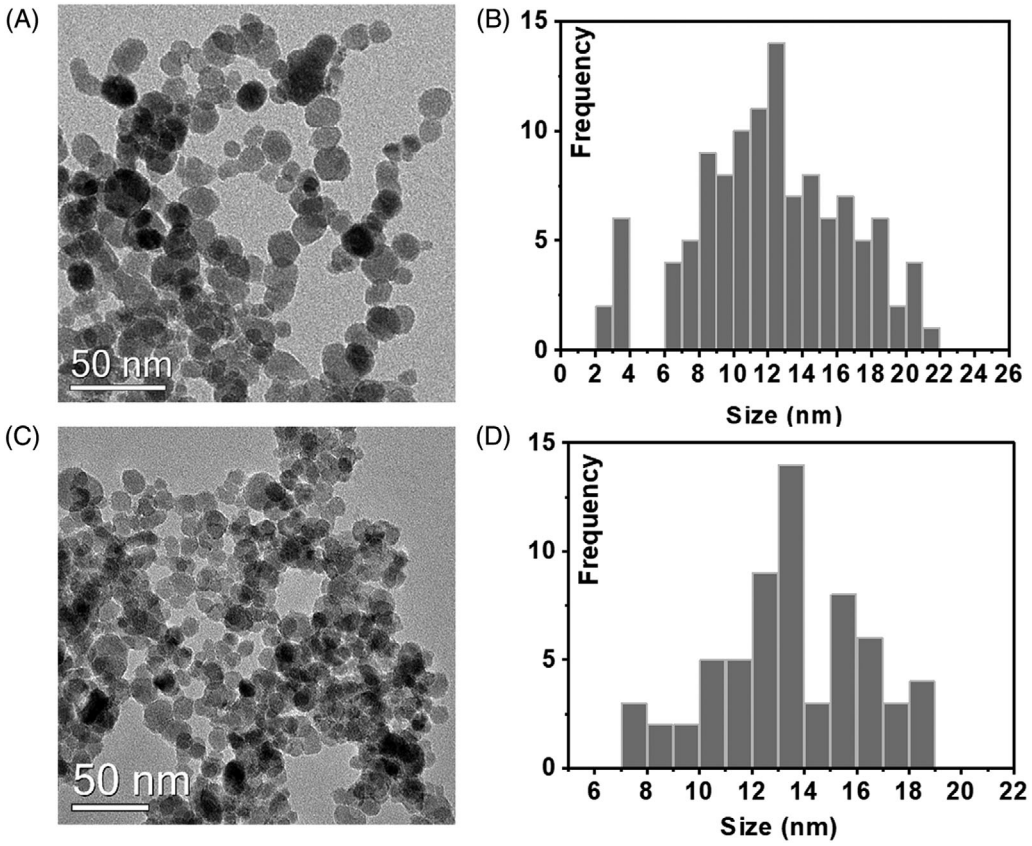

FIGURE 4 Transmission electron microscopy (TEM) image (4A) and graph size distribution (4B) of magnetic nanoparticles (MNPs); TEM image (4C) and graph size distribution (4D) of M-A NPs

comparison with M-A, this is due to its absence of APTES external coating that could affect this property. In fact, out of the total quantity, the magnetite will be much lower in the sample in which the APTES is also present, and this could lower the magnetic response. Anyway, both samples show no hysteresis, which is characteristic of superparamagnetic behaviour and confirms the nanometric size of MNPs.

The morphology and distribution size of MNPs and M-A NPs are reported in Figure 4. The TEM image of MNPs (Figure 4A) shows an approximately spherical shape and a size range between 10 and 15 nm as confirmed by the size distribution plot, which revealed an average diameter of 12 ± 4 nm (Figure 4B). As shown in TEM image (Figure 4C), the morphology was not affected by the addition of APTES, and the size distribution plot (Figure 4D) shows an average diameter of M-A NPs of 14 ± 3 nm.

3.2 | Characterization of composite nanoplatforms

Figure 5 reports the UV-Visible spectra and the STEM analysis of synthesis 1a, 2a, and 3a. In particular, in the synthesis 1a (Figure 5D) only few bright spots ascribable to GNPs on MNPs surface are visible, this could indicate that the $HAuCl_4$ reduction in the presence of the lower amount of APTES and without the action of a specific reducing agent only induced the nucleation of GNPs, and few of them reached the crytical radius to grow up to a size detectable with STEM analisys. This is also confirmed from UV-Vis spectra (Figure 5A), in which only a weak signal is visible in the typical gold absorbing window between 500 nm and 600 nm, as evidenced in figure. Similar results have been previously reported by the authors in a preliminar investigation.[22]

On the contrary, in synthesis 2a (Figure 5E) and synthesis 3a (Figure 5F), GNPs with bigger size are detected in both STEM images, and their presence is also confirmed by the UV-Vis analysis (Figure 5B,C respectively), which shows in both cases a strong signal in the gold absorbing range. In particular, the nanoplatforms obtained in synthesis 2a gave rise to an intense peak of absorption centered in corresponsdance of the gold absorbing window, while for the nanoplatforms obtained in synthesis 3a, a broader peak with a sort of plateau was recorded, according to the presence, in this case, of some rod-shaped GNPs together with spherical ones with heterogeneous dimension.[32,33]

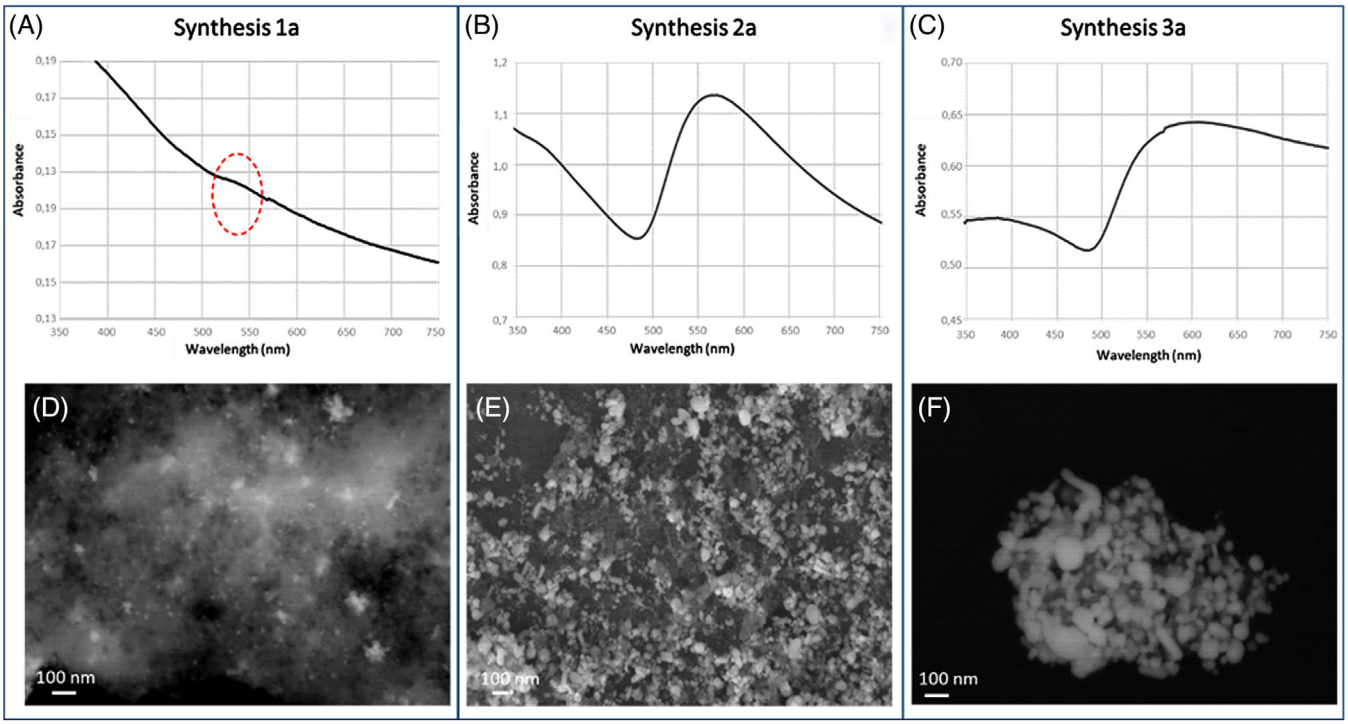

FIGURE 5 UV-visible spectra of samples obtained with synthesis 1a (A), synthesis 2a (B), and synthesis 3a (C). Scanning and transmission electron microscopy (STEM) images of samples obtained with synthesis 1a (D), synthesis 2a (E), and synthesis 3a (F)

According to the literature,[32–34] the optical properties of plasmonic NPs can be tuned by controlling the size of gold NPs and thus the synthesis parameters and particles funcionalization. However, the synthesis of magneto-plasmonic NPs with controllable size remains a great challenge.

Figure 6 shows the UV-visible spectra and STEM analysis of the nanoplatforms obtained with synthesis 1b, 2b, and 3b. The synthesis 1b shows only few spots ascribable to GNPs (Figure 6D) confirmed in the UV-Vis spectrum (Figure 6A), in which it is not possible to observe a well-defined peak but a slight curvature in the typical absorbing range. As previously observed, the absence of a specific reducing agent probably leads only to the nucleation of Au NPs, and few of them were able to grow. On the contrary, in synthesis 2b and 3b, a higher concentration of GNPs reached the critical size, as confirmed also by the UV-Vis analysis showed in Figure 6B,C, in which it is possible to observe in both cases a high signal in the GNPs absorbing window. The wide curve generated from synthesis 2b is probably due to the heterogeneous shape of GNPs as visible in the STEM image (Figure 6E), as already observed for synthesis 3a. We cannot explain, with the data collected in this work, the reason of the growth of some rod-shaped GNPs randomly observed in presence of TA, but this issue seems likely to be related to local fluctuations in the reagent concentrations, rather than to the sequence of chemicals addiction, in consideration that various factors, including molar ratio of metal salts to TA, have been found in literature to play a role in the generation of NPs of various shapes.[35]

TEM analysis was performed on the samples obtained with synthesis 1b, 2b, and 3b in which the higher amount of APTES was used for the functionalization (Figure 7A-C). All the figures confirm the composite nature of the obtained nanoplatforms: Figure 7A, related to synthesis 1b, shows few dark particles ascribable to GNPs with a homogeneous dimension below 10–15 nm and lots of spots even smaller, whose dimension is difficult to be assessed, probably under 5 nm (as evidenced in figure); Figure 7B confirms the STEM results of the synthesis 2b showing the heterogeneous shape and dimension up to 100 nm of GNPs; Figure 7C shows homogenous shape and dimension around 20 nm of GNPs with some exception of larger particles that can reach 100 nm.

In summary, the nanoplatform morphologies reported in Figures 5, 6, and 7 are consistent with the optical properties detected by UV-visible measurements. The very low (almost absent) absorption curve for the samples obtained without reducing agent (synthesis 1a and 1b), in particular for lower APTES functionalization (synthesis 1a) can be due both to the GNPs small size, undetected by STEM observation but visible by TEM observation on sample 1b, and to the low concentration of GNPs above the critical size to give plasmon signals: it is well known that for NPs smaller than 5 nm the plasmon oscillation is

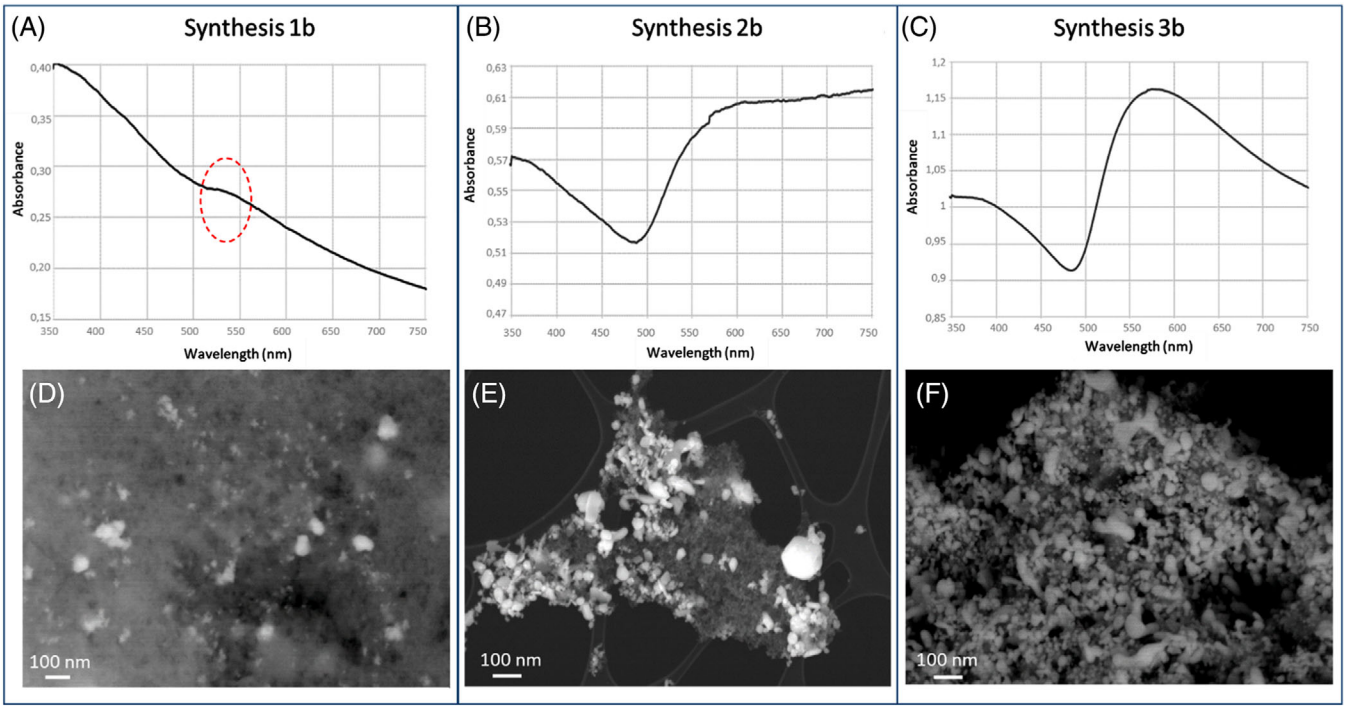

FIGURE 6 UV-visible spectra of samples obtained with synthesis 1b (A), synthesis 2b (B) and synthesis 3b (C). Scanning and transmission electron microscopy (STEM) images of samples obtained with synthesis 1b (D), synthesis 2b (E) and synthesis 3b (F)

strongly damped, resulting in a broad and low intensity plasmon signal.[36] On the contrary, samples 2a, 3a, 2b, and 3b revealed high amounts of GNPs with size and distribution correlated to a more intense peak in the absorption spectra or a plateau.[32,33,37–40]

The magnetic response measurements of nanoplatforms obtained with syntheses 1a, 2a, and 3a and those related to syntheses 1b, 2b, and 3b are reported in Figure 8A,B, respectively. In particular, in both images, the red curves are related to the syntheses in which the $Au(OH)_3$ seeds were directly added to the M-A NPs suspension without using TA as reducing agent; the green curves are related to the syntheses in which $HAuCl_4$ and TA solutions were pre-mixed together and then added to the M-A NPs suspension; the blue curves are related to the syntheses performed adding $HAuCl_4$ and TA in sequence to the M-A NPs suspension. In both Figure 8A,B, all the samples show no hysteresis, no remanence, or coercivity, which is in agreement with superparamagnetic behavior of magnetite. All samples show a magnetic response, evidencing a decrease in saturation magnetization respect the bare MNPs and M-A NPs, probably due in part to the presence of APTES and, above all, to the diamagnetic nature of gold (saturation magnetization is given by the mass of the whole sample). The NPs obtained using the greatest amount of APTES (syntheses 1b, 2b, and 3b) show the same trend of synthesis 1a, 2a, and 3a, but with a more pronounced decrease of Ms. This result can be explained considering the great affinity that amine groups have to gold NPs and their ability to immobilize them through electrostatic interactions.[41,42]

It is also evident that among the three synthesis conditions, both for Figure 8A than for 8B, the higher saturation magnetization is presented by the sample in which $Au(OH)_3$ suspension and TA solution were pre-mixed together and then added to the M-A NPs suspension (syntheses 2a and 2b), the intermediate one is presented by the samples in which $HAuCl_4$ and TA solutions were added to the MNPs suspension in sequence (syntheses 3a and 3b), and the lowest one is presented by the samples in which no TA has been used (syntheses 1a and 1b). This trend is particularly evident for syntheses b (the ones in which the highest amount of APTES has been used for the functionalization of MNPs).

As said before, the decrease in the magnetic response could be generically attributed to the increase in the weight ratio of gold, as a consequence of GNPs loading on MNPs. The above reported particular trend of the Ms values could be related to a different yield of a reaction of the various reduction mechanisms, as follows.

Samples obtained by syntheses 1a and 1b are mainly characterized by very small GNPs, not able to produce a sharp plasmon signal, but able to strongly weaken the magnetization. Their fast nucleation is explainable, as reported in a previous work,[22] taking into account that during the early stages of the synthesis, the $HAuCl_4$ hydrolysis takes

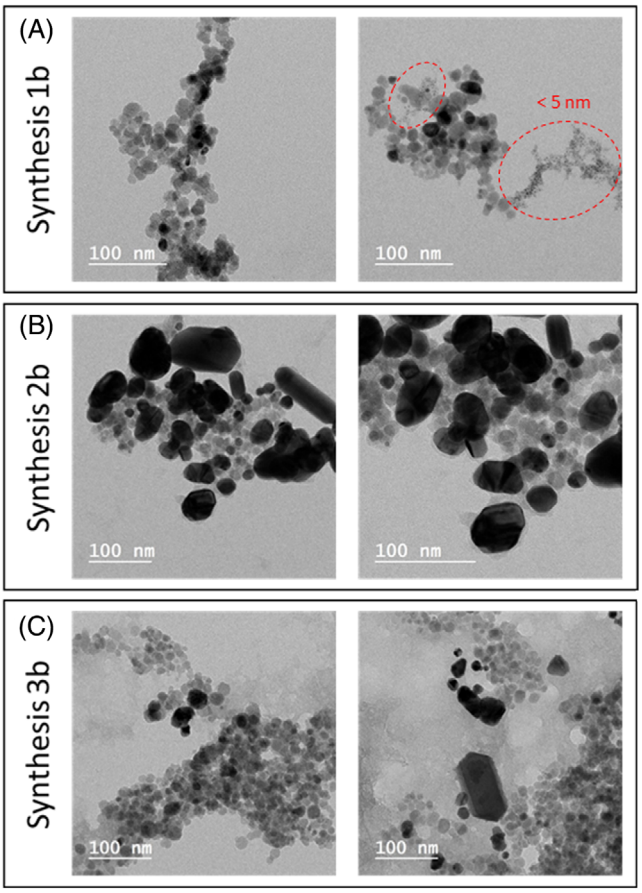

FIGURE 7 Transmission electron microscopy (TEM) images of synthesis 1b (A), synthesis 2b (B), and synthesis 3b (C)

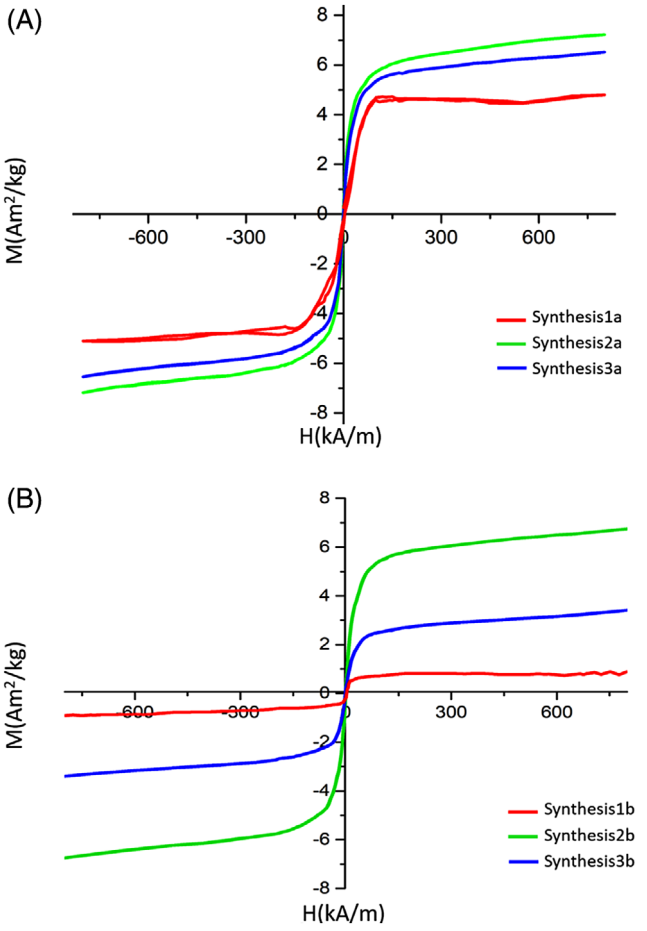

FIGURE 8 Magnetic measurement of sample 1a, 2a, and 3a (A) and sample 1B, 2B, and 3B (B)

place to form lots of gold hydroxide seeds ($Au(OH)_3$), which are strongly attracted by the amine groups on the surface of APTES-functionalized MNPs. Without the use of TA as reducing agent, the reduction of these numerous $Au(OH)_3$ seeds to metallic GNPs can only be weakly promoted by the reaction environment, such as by the hydroxyl groups of ethanol, or by Fe II ions, as well as by the CA used to improve the MNPs suspension stability, so many GNPs nucleate, but their growth is hampered. For this reason, samples 1a and 1b show very weak plasmon signals (due to small size of GNPs) and a very strong reduction of Ms (due to their fast nucleation in contact with the MNPs). Due to the poor SPR response and the negative effect on the magnetic properties, these syntheses are considered the less promising.

In syntheses 2a and 2b, the reduction of GNPs takes place in the solution before seeding on the MNPs, because the $HAuCl_4$ hydrolysis to form $Au(OH)_3$ seeds is concurrent with the addition of TA. So the nucleation of GNPs competes with their growth due to the presence of a strong reducing agent, and only after this step they are exposed to the amine groups of APTES-functionalized MNPs. In these conditions, since the $Au(OH)_3$ seeds are not exposed directly to the MNPs surface, the obtained nanoplatforms originate from the attraction of already formed GNPs by the APTES-functionalized MNPs, being able to give a strong plasmon signal (due to their high dimensions), without hampering the Ms of the MNPs (since they are not originated in direct contact with MNPs). Although both SPR effect and magnetic response are not negatively affected, these syntheses produced very large and heterogeneous nanoplatforms, due to a nucleation and growth of GNPs not mediated by the MNPs surface. However, in future works, the size of GNPs could be optimized by varying the chloroauric acid/TA ratio.

In the synthesis 3a and 3b, an intermediate behavior is plausible, since the sequential addition of $Au(OH)_3$ and TA let suppose that, at first, $Au(OH)_3$ clusters are attracted on the APTES-functionalized MNPs surface, and the nucleation of GNPs starts on it, but it is suddenly overcome by the addition of TA, which promotes their growth. In this case, the obtained nanoplatforms are able to give a strong plasmon signal (due to the GNPs size), hampering only in a moderate way the Ms of the MNPs, since the metallic GNPs nucleate on the MNPs in competition with

their growth. In these syntheses, a more controlled nucleation and growth of GNPs takes place on the surface of MNPs, resulting in more homogeneous size and shape and the best compromise between plasmonic and magnetic properties.

In summary, the obtained results confirm that the use of TA as a reducing agent allowed a fast growth of GNPs. This is true both for the synthesis in which $Au(OH)_3$ colloidal suspension was previously mixed with TA and for the synthesis in which $Au(OH)_3$ and TA were added in sequence, but only in the second case, the nucleation and growth of the GNPs took place on the surface of the MNPs, affecting the magnetic response. The syntheses in which TA was not used produced nanoplatforms with highly hindered Ms and very weak plasmon signals.

4 | CONCLUSIONS

This work was aimed to develop magneto-plasmonic heterodimers made of MNPs-GNPs composite nanoplatforms, obtained by MNPs co-precipitation synthesis followed by dispersion in CA, APTES functionalization and grafting with GNPs, for a potential use in cancer theranostics. A specific challenge was to immobilize GNPs onto chemically modified surface of MNPs using or not TA as reducing agent, in order to obtain well dispersed M-A-Au nanocomposites, with both magnetic and plasmonic properties. In particular, the work was focused on the investigation of the influence, on the final nanocomposite properties, of various synthesis parameters, such as the APTES amount and the different sequences of addition of TA as reducing agent for GNPs precursors.

Indeed, the functionalization with APTES allowed the grafting of GNPs onto previously dispersed CA-M NPs. The morphological characterization confirmed that the shape and dimensions of M-A-Au nanocomposites can be tuned by the concentration of APTES used for the functionalization, which assure the GNPs grafting to the MNPs surface, as well as by the use of TA as reducing agent, which promotes the growth of GNPs. Moreover, it was demonstrated that the sequence of addition of the GNPs precursors and of the TA is crucial to guide the nucleation and growth of GNPs, tailoring their size and shape and, in turn, the magneto-plasmonic properties of the obtained nanoplatforms, which were able to maintain the peculiar properties of both the GNPs and the MNPs.

It is possible to attest that in order to maintain the peculiar properties of both the GNPs and the MNPs and to exploit the gold absorbing peak in the specific gold absorbing range, while maintaining the superparamagnetic behavior typical of the magnetite NPs, a proper optimization of the synthesis steps should be planned, taking into account the role of MNPs surface (functionalized with APTES) as preferential site of GNPs nucleation and growth. Furthermore, it can also be assessed that the APTES amount used for the MNPs functionalization can significantly influence the fate of the process, in terms of magnetic properties of the heterodimers, amplifying the differences among the various synthesis routes.

ACKNOWLEDGMENTS

This work was self-funded, thanks to the Assignments for Basic Research (2017-2020) provided by Politecnico di Torino.

Open Access Funding provided by Politecnico di Torino within the CRUI-CARE Agreement.

ORCID

Marta Miola https://orcid.org/0000-0002-1440-6146
Enrica Vernè https://orcid.org/0000-0002-8649-4739

REFERENCES

1. Kargozar S, Mozafari M. Nanotechnology and Nanomedicine: Start small, think big. *Mater*. Today Proc. 2018;5:15492–500.
2. Siddique S, Chow JCL. Application of nanomaterials in biomedical imaging and cancer therapy. Nanomaterials 2020;10:1700.
3. Zhang Y, Li M, Gao X, Chen Y, Liu T. Nanotechnology in cancer diagnosis: progress, challenges and opportunities. J Hematol Oncol. 2019;12:1–13.
4. Khan I, Saeed K, Khan I. Nanoparticles: properties, applications and toxicities. Arab J Chem. 2019;12:908–31.
5. Chen F, Ehlerding EB, Cai W. Theranostic nanoparticles. J Nucl Med. 2014;55:1919–22.
6. Revia RA, Zhang M. Magnetite nanoparticles for cancer diagnosis, treatment, and treatment monitoring: recent advances. Mater Today. 2016;19:157–68.
7. Mukherjee S, Liang L, Veiseh O. Recent advancements of magnetic nanomaterials in cancer therapy. Pharmaceutics 2020;12:147.
8. Fathi Karkan S, Mohammadhosseini M, Panahi Y, Milani M, Zarghami N, Akbarzadeh A, et al. Magnetic nanoparticles in cancer diagnosis and treatment: a review. Artif Cells Nanomed Biotechnol. 2017;45:1–5.
9. Samrot AV, Sahithya CS, Selvarani J, Purayil SK, Ponnaiah P. A review on synthesis, characterization and potential biological applications of superparamagnetic iron oxide nanoparticles. Curr Res Green Sustainable Chem. 2020;4:100042.
10. Pang X, Zhao L, Han W, Xin X, Lin Z. A general and robust strategy for the synthesis of nearly monodisperse colloidal nanocrystals. Nat Nanotechnol. 2013;8:426–31.
11. Pang X, He Y, Jung J, Lin Z. 1D nanocrystals with precisely controlled dimensions, compositions, and architectures. Science. 2016;353:1268–72.
12. Bai X, Wang Y, Song Z, Feng Y, Chen Y, Zhang D, et al. The basic properties of gold nanoparticles and their applications in tumor diagnosis and treatment. Int J Mol Sci. 2020;21:2480.
13. Seino S, Kusunose T, Sekino T. Synthesis of gold/magnetic iron oxide composite nanoparticles for biomedical applications with good dispersibility. J Appl Phys. 2006;99:08H101.

14. Sebastian V, Calatayud MP, Goya GF, Santamaria J. Magnetically-driven selective synthesis of Au clusters on Fe 3 O 4 nanoparticles. Chem Commun. 2013;49:716–8.
15. León Félix L, Sanz B, Sebastián V, Torres TE, Sousa MH, Coaquira JAH, et al. Gold-decorated magnetic nanoparticles design for hyperthermia applications and as a potential platform for their surface-functionalization. Sci Rep. 2019;9:4185.
16. Sun H, Jiao X, Han Y, Jiang Z, Chen D. Synthesis of Fe3O4-Au nanocomposites with enhanced peroxidase-like activity. Eur J Inorg Chem. 2013;2013:109–14.
17. Yan F, Sun R. Facile synthesis of bifunctional Fe3O4/Au nanocomposite and their application in catalytic reduction of 4-nitrophenol. Mater Res Bull. 2014;57:293–9.
18. Zhu N, Ji H, Yu P, Niu J, Farooq MU, Waseem Akram M, et al. Surface modification of magnetic iron oxide nanoparticles. Nanomaterials 2018;8:810.
19. Nguyen TT, Mammeri F, Ammar S. Iron oxide and gold based magneto-plasmonic nanostructures for medical applications: a review. Nanomater (Basel). 2018;8:149.
20. Sood A, Arora V, Shah J, Kotnala RK, Jain TK. Ascorbic acid-mediated synthesis and characterisation of iron oxide/gold core–shell nanoparticles. J Exp Nanosci. 2016;11:370–82.
21. Norouz Dizaji A, Yilmaz M, Piskin E. Silver or gold deposition onto magnetite nanoparticles by using plant extracts as reducing and stabilizing agents. Artif Cells Nanomed Biotechnol. 2016;44:1109–15.
22. Miola M, Ferraris S, Pirani F, Multari C. Reductant-free synthesis of magnetoplasmonic iron oxide-gold nanoparticles. Ceram Int. 2017;43:15258–65.
23. Multari 1 C, Miola M, Laviano F, Gerbaldo R, Pezzotti G, Debellis D, et al. Magnetoplasmonic nanoparticles for photothermal therapy. Nanotechnology 2019;30:255705.
24. Borroni E, Miola M, Ferraris S, Ricci G, Ž Rožman K, Kostevšek N, et al. Tumor targeting by lentiviral vectors combined with magnetic nanoparticles in mice. Acta Biomater. 2017;59:303–16.
25. Multari C, Miola M, Ferraris S, Movia D, Ž Rožman K, Kostevšek N, et al. Synthesis and characterization of silica-coated superparamagnetic iron oxide nanoparticles and interaction with pancreatic cancer cells. Int J Appl Ceram Technol. 2018;15:947–60.
26. Campelj S, Makovec D, Drofenik M. Preparation and properties of water-based magnetic fluids. J Phys Condens Matter. 2008;20:204101.
27. Bini RA, Marques RFC, Santos FJ, Chaker JA, Jafelicci Jr M. Synthesis and functionalization of magnetite nanoparticles with different amino-functional alkoxysilanes. J Magn Magn Mater. 2012;324:534–9.
28. Yamaura M, Camilo RL, Sampaio LC, Macêdo MA, Nakamura M, Toma HE. Preparation and characterization of (3-aminopropyl)triethoxysilane-coated magnetite nanoparticles. J Magn Magn Mater. 2004;279:210–7.
29. Răcuciu M, Creanga D, Airinei A. Citric-acid-coated magnetite nanoparticles for biological applications. Eur Phys J E Soft Matter. 2006;21:117–21.
30. Liu Y, Li Y, Li X-M, He T. Kinetics of (3-Aminopropyl) triethoxylsilane (APTES) Silanization of Superparamagnetic Iron Oxide Nanoparticles. Langmuir 2013;29:15275–82.
31. Majoul N, Aouida S, Bessaïs B. Progress of porous silicon APTES-functionalization by FTIR investigations. Appl Surf Sci. 2015;331:388–91.
32. Kim HS, Lee DY. Near-infrared-responsive cancer photothermal and photodynamic therapy using gold nanoparticles. Polymers 2018;10:961
33. cytodiagnostics Introduction to gold nanoparticle characterization. Available from: https://www.cytodiagnostics.com/pages/introduction-to-gold-nanoparticle-characterization. Accessed 22 Oct 2021.
34. Yang D, Pang X, He Y, Wang Y, Chen G, Wang W, et al. Precisely size-tunable magnetic/plasmonic core/shell nanoparticles with controlled optical properties. Angew Chemie. 2015;127:12259–64.
35. Ahmad T. Reviewing the tannic acid mediated synthesis of metal nanoparticles. J Nanotechnol. 2014;2014:954206.
36. Selvan ST, Nogami M, Nakamura A, Hamanaka Y. A facile sol–gel method for the encapsulation of gold nanoclusters in silica gels and their optical properties. J Non Cryst Solids. 1999;255:254–8.
37. Nanocomposix Gold nanoparticles: optical properties. Available from: https://nanocomposix.com/pages/gold-nanoparticles-optical-properties#target. Accessed 22 Oct 2021.
38. Li R, Gu X, Liang X, Hou S, Hu D. Aggregation of gold nanoparticles caused in two different ways involved in 4-mercaptophenylboronic acidand hydrogen peroxide. Materials (Basel). 2019:12:1802.
39. Steckiewicz KP, Barcinska E, Malankowska A, Zauszkiewicz-Pawlak A, Nowaczyk G, Zaleska-Medynska A, et al. Impact of gold nanoparticles shape on their cytotoxicity against human osteoblast and osteosarcoma in in vitro model. Evaluation of the safety of use and anti-cancer potential. J Mater Sci Mater Med. 2019;30:22.
40. López-Muñoz GA, Pescador-Rojas JA, Ortega-Lopez J, Salazar JS, Balderas-López JA. Thermal diffusivity measurement of spherical gold nanofluids of different sizes/concentrations. Nanoscale Res Lett. 2012;7:423.
41. Rak MJ, Saadé NK, Friščić T, Moores A. Mechanosynthesis of ultra-small monodisperse amine-stabilized gold nanoparticles with controllable size. Green Chem. 2014;16:86–9.
42. Ben Haddada M, Blanchard J, Casale S, Krafft JM, Vallée A, Méthivier C, et al. Optimizing the immobilization of gold nanoparticles on functionalized silicon surfaces: amine- vs thiol-terminated silane. Gold Bull. 2013;46:335–41.

How to cite this article: Miola M, Multari C, Debellis D, Laviano F, Gerbaldo R, Vernè E. Magneto-plasmonic heterodimers: Evaluation of different synthesis approaches. J Am Ceram Soc. 2022;105:1276–1285.
https://doi.org/10.1111/jace.18190